Eur Radiol (2009) 19: 745–760
DOI 10.1007/s00330-008-1185-5

UROGENITAL

Tomohiro Namimoto
Kazuo Awai
Takeshi Nakaura
Yumi Yanaga
Toshinori Hirai
Yasuyuki Yamashita

Role of diffusion-weighted imaging in the diagnosis of gynecological diseases

Received: 11 June 2008
Revised: 6 August 2008
Accepted: 30 August 2008
Published online: 7 October 2008

T. Namimoto (✉) · K. Awai ·
T. Nakaura · Y. Yanaga · T. Hirai ·
Y. Yamashita
Department of Diagnostic Radiology,
Graduate School of Medical Sciences,
Kumamoto University,
1–1–1, Honjo,
Kumamoto, 860–8556, Japan
e-mail: namimottoo@yahoo.co.jp
Tel.: +81-96-3735261
Fax: +81-96-3624330

Abstract Recent technical advances in diffusion-weighted imaging (DWI) greatly enhanced the clinical value of magnetic resonance imaging (MRI) of the body. DWI can provide excellent tissue contrast based on molecular diffusion and may be able to demonstrate malignant tumors. Quantitative measurement of the apparent diffusion coefficient (ADC) may be valuable in distinguishing between malignant and benign lesions. We reviewed DWI and conventional MRI of the female pelvis to study the utility of DWI in patients with gynecological diseases. Although the ADC can help to differentiate between normal and cancerous tissue in the uterine cervix and endometrium, its utility may be limited by the large overlap of the uterine myometrium and ovaries. On the other hand, the ADC may be useful for monitoring the therapeutic outcome after uterine arterial embolizati (UAE), chemotherapy and/or radiation therapy. In patients with ovarian cancer, DWI demonstrates high intensity not only at the primary cancer site but also in disseminated peritoneal implants. When added to conventional MRI findings, DWI and ADC values provide additional information and DWI may play an important role in the diagnosis of patients with gynecological diseases.

Keywords Diffusion · ADC · Magnetic resonance imaging · Uterus · Ovary

Introduction

Although diffusion-weighted imaging (DWI) now plays an important role in the diagnosis of brain disorders [1–3], it has not been fully applied to body imaging because the images become distorted by its sensitivity, resulting in misregistration attributable to chemical-shift artifacts. Advances in parallel imaging techniques have reduced image distortion and increased the signal-to-noise ratio (SNR), rendering body DWI feasible [4]. DWI can demonstrate abnormal signals emitted by pathologic foci based on differences in molecular diffusion. It also permits the quantitative evaluation of the apparent diffusion coefficient (ADC) that may be useful for distinguishing between malignant and benign tissues and for monitoring therapeutic outcomes [5–11]. As there are few studies on the utility of DWI for gynecological imaging [12–26], we reviewed its applicability for examining the female pelvic region and discuss the future of MRI in patients with gynecological diseases.

Examination of the female pelvic region using DWI

DWI is obtained by measuring signal loss after a series of two motion-providing gradient (MPG) pulses added to both sides of a 180° refocusing RF pulse to enhance differences in molecular diffusion between tissues. DWI with echo-planar imaging (EPI) can yield an excellent contrast-to-noise ratio (CNR), because the signal of most organs is very low while that of lesions is high. The intensity of MPG pulses is represented by the *b*-value, an important parameter that affects the signal intensity on DWI. DWI with an intermediate *b*-value (e.g., 500 s/mm^2) show increased intensity not only in tumors but also in ascites. Since the signal intensity on DWI can be

influenced by the signal intensity on T2-weighted images (T2-WI), high-intensity tissues on T2-WI may exhibit increased signal intensity on DWI (the so-called T2 "shine-through" effect) [27, 28]. Thus, DWI with a higher *b*-value (e.g., 800 or 1,000 s/mm^2) may be required for the female pelvic region. In body regions, optimization of other sequence parameters is crucial, since EPI is highly susceptible to distortions in the spatial field due to air-containing bowel loops. To minimize susceptibility artifacts, shorter echo times (TE) and smaller numbers of echo train lengths (ETLs) are preferable; this can be achieved by the use of parallel imaging techniques. Unlike sequential acquisitions, parallel imaging is based on the use of coils with multiple small detectors that operate simultaneously to acquire MR data. Each of these detectors contains spatial information that can be used as a substitute for time-consuming phase-encoding steps, thereby allowing both the acquisition time and the ETL to be reduced. In particular, DWI with parallel imaging reduces the number of phase-encoding steps, the effective TE can be shortened and susceptible components of the ETL can be eliminated. This keeps the susceptibility effect to a minimum. Although a wider receiver band-width reduces the SNR, its use is recommended because it shortens the MR signal acquisition duration and reduces susceptibility artifacts. In our standard protocols for pelvic DWI, we use a 3-T magnet unit (Achieva 3T, Philips Medical System), a six-channel SENSE body coil, and an EPI sequence (TR, 3,000–3,200 ms; TE, 37–40 ms; flip angle, 90°; field of view, 280 mm; two excitations; slice thickness, 5 mm; interslice gap, 1 mm; acquisition matrix 128 × 128; ETL, 37; and bandwidth 3,018 Hz/pixel) with a chemical shift selective (CHESS) fat suppression and parallel imaging technique (SENSE factor of 2). Imaging time of DWI was 90 s for 20 slices.

Detection of uterine malignancy

The ADC values of uterine cancers are lower than of normal tissue. On the other hand, in sarcomas the ADC may play a limited role due to a large overlap between sarcomas and benign leiomyomas (Table 1).

Uterine cervix

Vaginal access renders the detection and biopsy of uterine cervix tumors straightforward. For the diagnosis of tumor spread, conventional T1- and T2-WI provide fairly good information and dynamic contrast-enhanced images can provide details on tumor spread and vascularity (Fig. 1) [24, 29–34]. According to Naganawa et al. [12], the mean ADC value of cervical cancer lesions was lower than of normal cervical tissue (1.09×10^{-3} vs 1.79×10^{-3} mm^2/s); it returned to the normal range after chemotherapy and/or radiation therapy. However, this study showed, with a small number of patients (12 cervical cancers with nine chemotherapy and/or radiation therapy, ten controls). Further study using larger numbers of patients is needed to establish the accuracy of ADC measurement in monitoring the effect of therapy for uterine cervical cancer. For the diagnosis, McVeigh et al. [13] reported with larger

Table 1 DW studies with ADC values in uterine diseases

Authors of Study	Year of Publication	Journal	Tumour & Tissue (no. of subjects)	b-values	ADC (10^{-3} mm^2/s)
Naganawa S. et al. [12]	2004	Eur Radiol	cervical cancer (12)	0, 300, 600	1.09 ± 0.20
			normal cervix (10)		1.79 ± 0.24 *
McVeigh PZ. et al. [13]	2008	Eur Radiol	cervical cancer (47)	0, 600	1.09 ± 0.20
			normal cervix (26)		2.09 ± 0.46 *
Tamai K. et al. [14]	2007	J Magn Reson	endometrial cancer (18)	0, 500, 1000	0.88 ± 0.16
			Imaging normal endmetrium (12)		1.53 ± 0.10 *
Fujii S. et al. [15]	2007	Eur Radiol	endometrial cancer (11)	0, 1000	0.98 ± 0.21
			endometrial polyp (4)		1.58 ± 0.45 *
Shen SH. et al. [16]	2008	AJR	endometrial cancer (11)	0, 1000	1.86 ± 0.31
			endometrial polyp or hyperplasia (7)		1.27 ± 0.22 *
Tamai K. et al. [17]	2007	Eur Radiol	uterine sarcoma (7)	0, 500, 1000	1.17±0.15
			leiomyoma (51)		0.88±0.27
			normal myometrium		1.62±0.11

* $p<0.01$

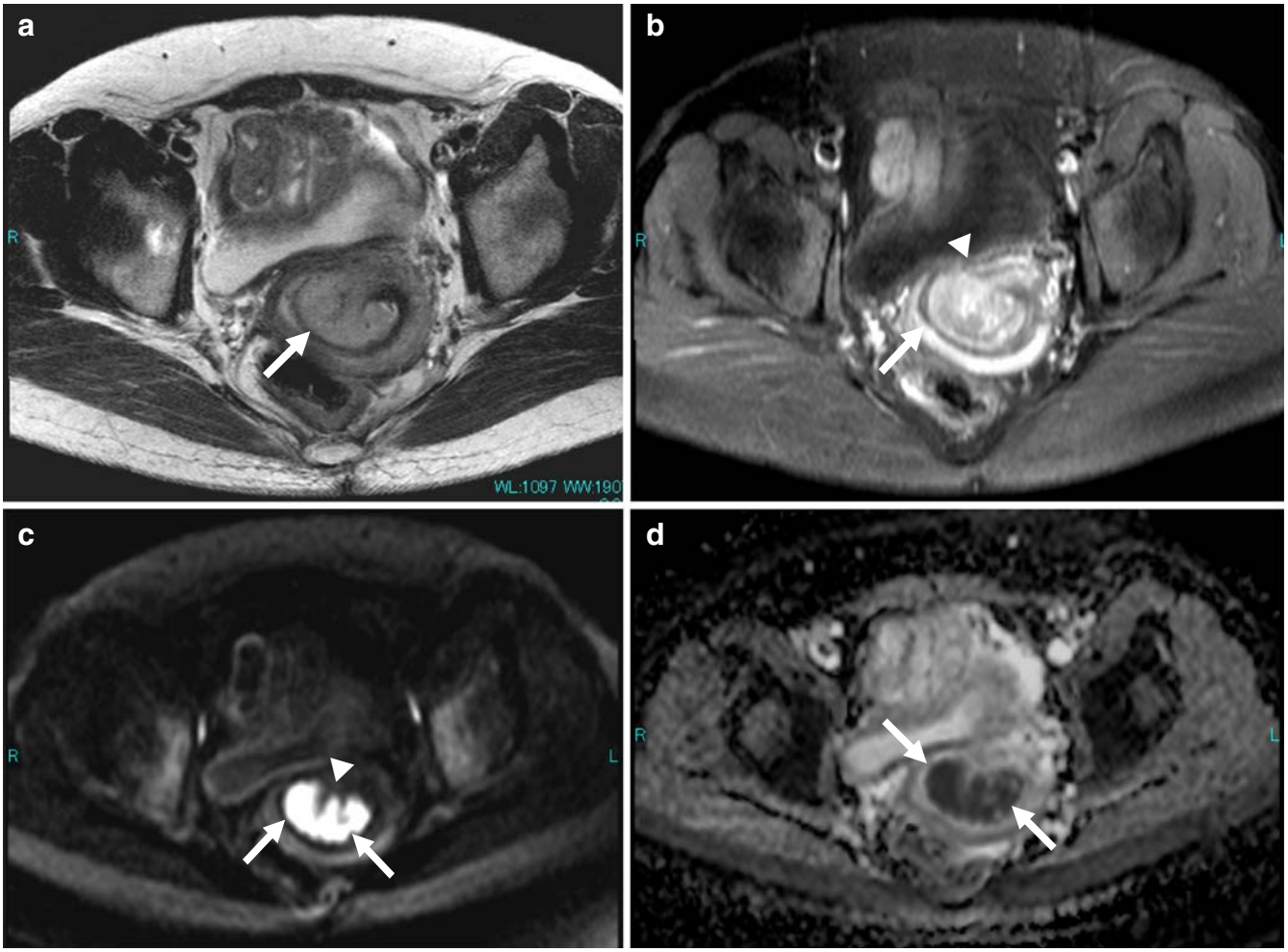

Fig. 1a–d A 44-year-old woman with stage Ib squamous cell carcinoma of the uterine cervix. **a** Axial T2-WI of the uterus shows cervical cancer (*arrow*) involving the anterior lip of the cervix. **b** Dynamic contrast-enhanced T1-WI with fat suppression shows a strongly enhancing cervical cancer (*arrow*). The tumor invades the cervical stroma (*arrowhead*). **c** DWI with b = 1,000 s/mm^2 shows a well-defined hyperintensity mass in the cervical area. The shape of the uterine cervix is distorted in the DWI (*arrowhead*). **d** On the ADC map the tumor is hypointense (*arrow*) and the normal cervix is hyperintense. Note that the contrast on the ADC map is opposite that seen on DWI with b = 1,000 s/mm^2. The ADC value within the mass is 0.67×10^{-3} mm^2/s

number of patients (47 cervical cancers, 26 normal cervix) that the average median ADC of cervical cancers was significantly lower than normal cervix (1.09×10^{-3} vs 2.09×10^{-3} mm^2/s). These studies suggested that ADC measurement has a potential ability to differentiate between normal and cancerous tissue in the uterine cervix. Further study into its predictive value for long-term outcome will determine the ultimate clinical utility.

Uterine endometrium

Endometrial cancer is usually demonstrated on T2-WI (Fig. 2). However, conventional MRI does not always demonstrate the tumor focus because the signal intensity of endometrial cancer ranges from high to low and is sometimes indistinguishable from normal endometrium or adjacent myometrium [34–38] Therefore, intravenous dynamic contrast enhancement is necessary at MRI study of endometrial carcinoma. The reported diagnostic accuracy of dynamic contrast-enhanced MRI is higher than of T2-WI (85–93% vs 58–77%) [24, 34–37]. DWI can demonstrate uterine endometrial cancer and the ADC may help to differentiate between benign and cancerous endometrial tissue (Figs. 2, 3). The ADC value of endometrial cancer ($0.88–0.98 \times 10^{-3}$ mm^2/s) is significantly lower than of endometrial polyps ($1.27–1.58 \times 10^{-3}$ mm^2/s) and of normal endometrium (1.53×10^{-3} mm^2/s)

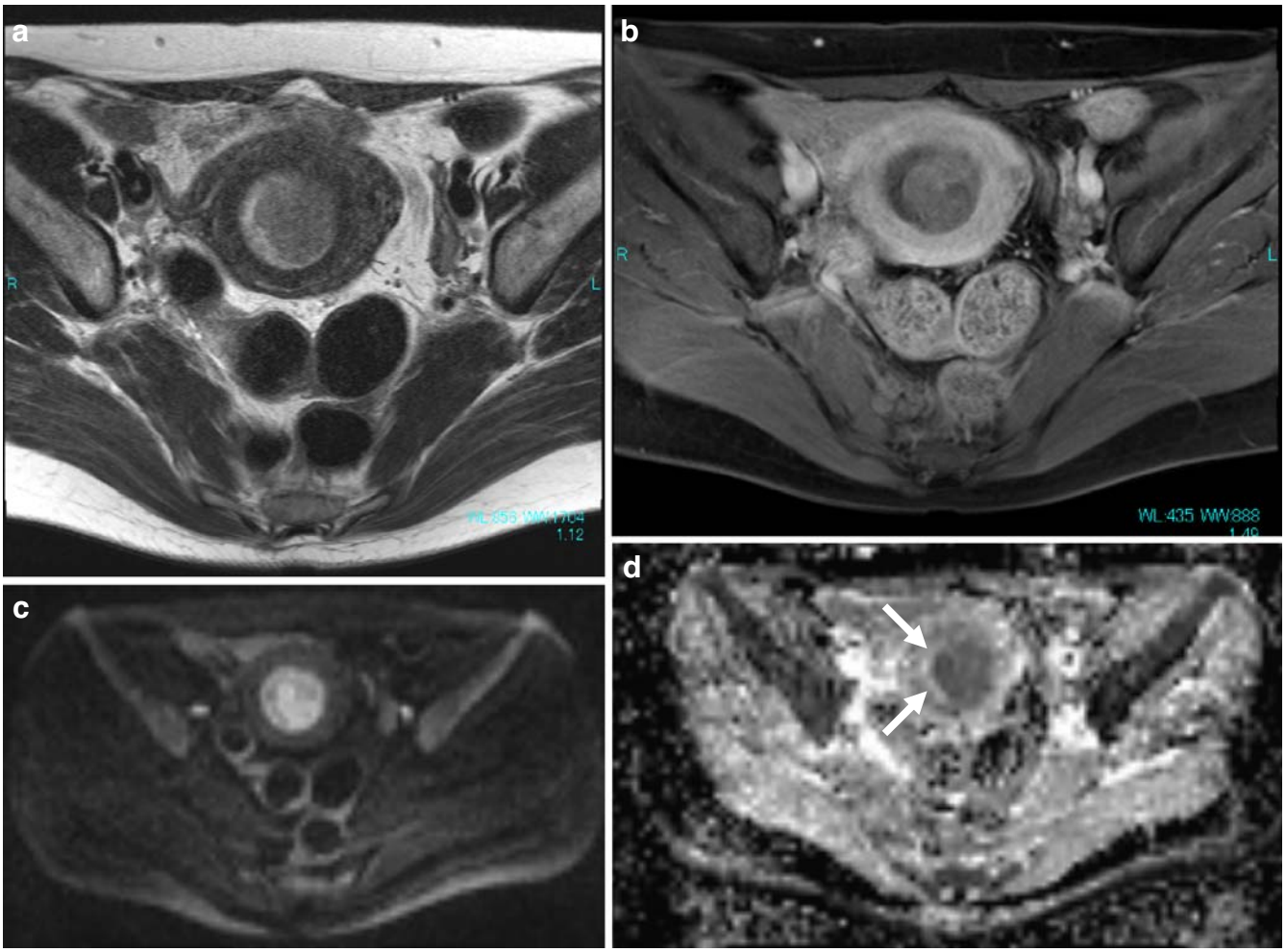

Fig. 2a–d A 52-year-old woman with grade 2 adenocarcinoma of the endometrium. **a** Axial T2-WI of the uterus shows intermediate signal intensity filling the endometrial cavity. **b** Contrast-enhanced T1-WI with fat suppression shows a weakly enhancing mass. The regular endometrial/myometrial interface suggests that the tumor is limited to the endometrium. **c** DWI with b = 1,000 s/mm^2 shows a well-defined high-signal intensity mass in the endometrial area. The hyperintense mass is clearly depicted on DWI with b = 1,000 s/mm^2. **d** ADC map demonstrates the tumor as hypointense and the normal endometrium as hyperintense (*arrows*). The ADC value within the mass is 0.81×10^{-3} mm^2/s

[14–16]. Tamai et al. [14] showed that there was no overlap between ADC values of endometrial cancers and those of normal endometrium. According to Fujii et al. [15], the diagnostic accuracy of the ADC was 84.6%. Shen et al. [16] reported that the diagnostic accuracy for myometrial invasion of DWI compared with gadolinium-enhanced T1-weighted 3D fat-suppressed spoiled gradient-recalled echo images in the same patients. The diagnostic accuracy for myometrial invasion was 61.9% for DWI and 71.4% for gadolinium-enhanced T1-weighted images. DWI has potential as a method for differentiating benign from malignant endometrial lesions. It also provides valuable information for preoperative evaluation and should be considered part of routine preoperative MRI evaluation for endometrial cancer. Further study using larger numbers of patients and long-term follow-up is needed to establish the accuracy of ADC measurement for uterine endometrial cancer.

Uterine myometrium

In order of frequency, malignant tumors of the myometrium are leiomyosarcoma and endometrial stromal

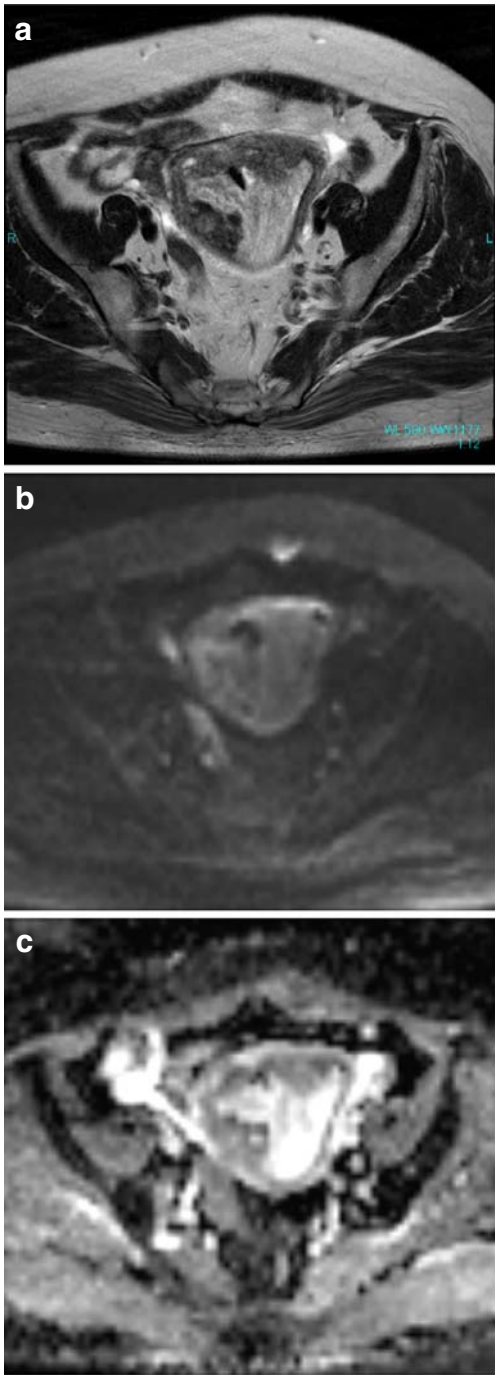

Fig. 3a–c A 71-year-old woman with endometrial polyps. **a** Axial T2-WI shows a mass with high signal intensity filling the endometrial cavity. **b** DWI with b = 1,000 s/mm^2 shows an ill-defined slightly hyperintense mass in the endometrial area. The DWI with b = 1,000 s/mm^2 shows marked signal loss in the endometrial area. **c** ADC map demonstrates the tumor as a heterogeneous hyperintensity. The ADC value within the mass is 1.76×10^{-3} mm^2/s

sarcoma [39]. On T2-WI MRI, uterine sarcomas often manifest intermediate to high signal intensity (Fig. 4) [38–42]. Although MRI usually yields a specific diagnosis of the much more common benign leiomyomas, they are occasionally associated with various types of degeneration or cellular histologic subtypes and this may result in increased signal intensity on T2-WI (Fig. 5). Therefore, the differentiation between benign and malignant myometrial tumors on non-enhanced and post-contrast MRI sequences may be difficult [38–48]. Tamai et al. [17] reported that DWI may be an additional tool for distinguishing uterine sarcomas from benign leiomyomas. The ADC values ($\times 10^{-3}$ mm^2/s) of uterine sarcomas (1.17) were lower than those of the normal myometrium (1.62) and degenerated leiomyomas (1.70) without any overlap; however, they were overlapped with those of ordinary leiomyomas (0.88) and cellular leiomyomas (1.19) (Figs. 4, 5). Because ordinary leiomyomas tend to contain hyalinized collagen, the signal intensity of ordinary leiomyomas is hypointensity on T2-weighted images. DWI can be explained with "T2 blackout effect", which indicates hypointensity on DWI caused by hypointensity on T2-WIs, resulting in a decrease in the ADC of ordinary leiomyomas [28]. ADC measurement may have a limited role due to a large overlap between sarcomas and benign leiomyomas. Leapi et al. [19] showed that the mean ADC value of leiomyomas (n = 32) was 1.74×10^{-3} mm^2/s before uterine arterial embolization (UAE) treatment, and significantly decreased to 1.22×10^{-3} mm^2/s after treatment. Jacob et al. [18] showed DW imaging and ADC mapping are feasible for identification of ablated tissue after focused ultrasound treatment of uterine leiomyomas (n = 14). Posttreatment ADC values for nontreated leiomyomas significantly differed from posttreatment ADC values for leiomyomas (1.68×10^{-3} vs 1.08×10^{-3} mm^2/s). A significant difference between ADC values for nontreated and treated (1.44×10^{-3} vs 1.91×10^{-3} mm^2/s), at 6-month follow-up was observed. The ADC value may also have a role in monitoring therapeutic outcomes after UAE or focused ultrasound ablation [18, 19].

Differentiation of ovarian tumors

There are some reports about the clinical application of DWI to diagnose cystic ovarian tumors (Table 2) [21–23]. The cystic components of endometrial cysts and malignant ovarian cystic tumors exhibited lower ADC values than other benign ovarian cysts without bleeding and benign cystic neoplasms (Figs. 6, 7, 8) [21, 22]. However, there is controversy regarding the usefulness of this technique in cystic ovarian tumors, particularly as applied to differentiating benign from malignant lesions. Nakayama et al. [23] applied to 131 cystic ovarian masses and assessed their

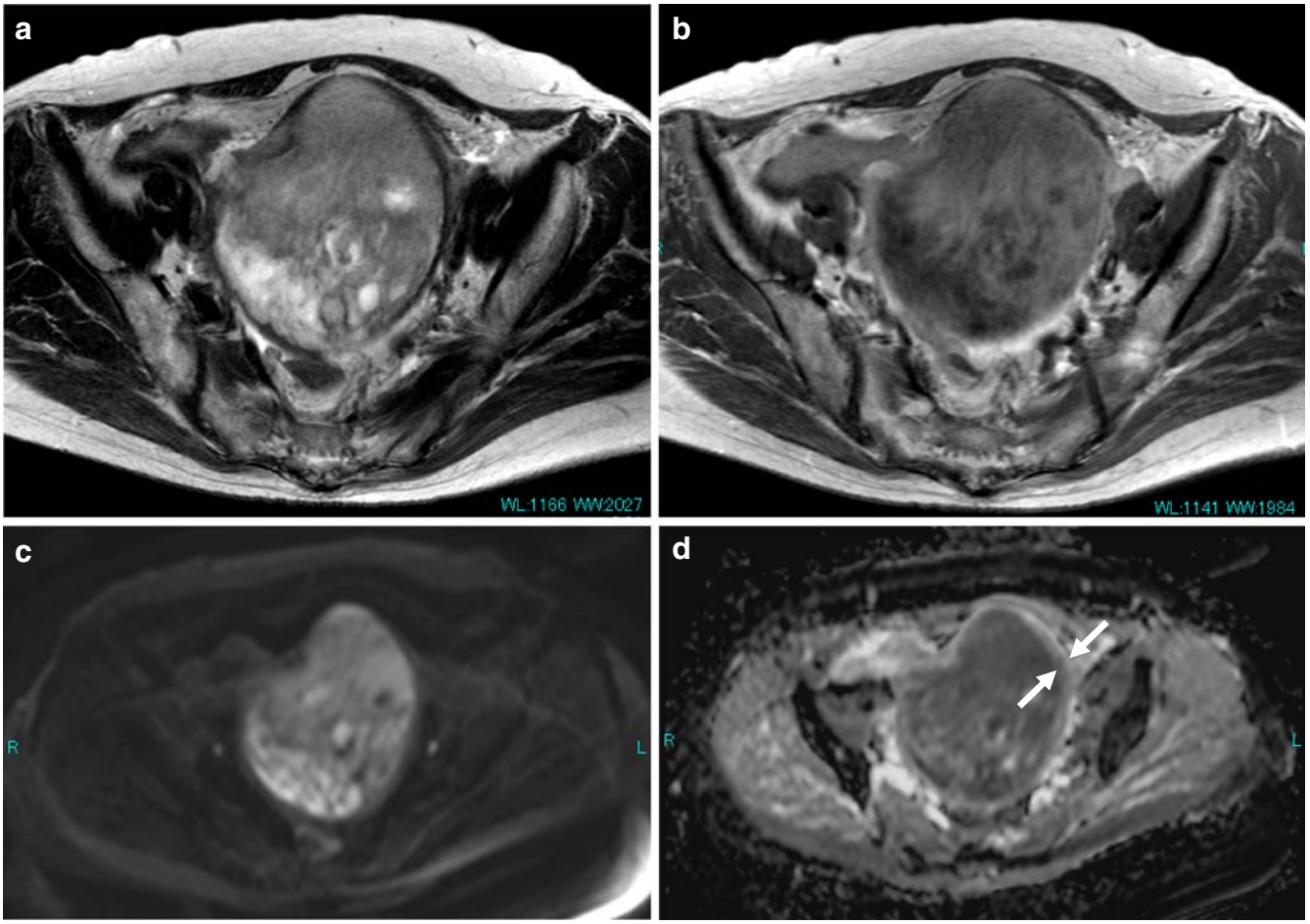

Fig. 4a–d A 78-year-old woman with leiomyosarcoma of the myometrium. **a** Axial T2-WI shows an ill-defined myometrial mass of heterogeneous high signal intensity invading the endometrial cavity. **b** Post-contrast axial T1-WI shows heterogeneous enhancement within the tumor. **c** DWI with $b = 1{,}000$ s/mm^2 demonstrates a hyperintensity mass. **d** ADC map demonstrates the tumor as hypointensity and the normal myometrium as hyperintensity (*arrow*). The ADC value within the mass is 0.87×10^{-3} mm^2/s

potential usefulness in the differential diagnosis. The cystic components of mature cystic teratomas had significantly lower ADC values than endometrial cysts, malignant neoplasms, and benign neoplasms. Differences between endometrial cysts and neoplasms, whether malignant or benign, were also significant. No significant difference in the ADC value was seen between benign and malignant cystic neoplasms. Because endometrial cysts tend to contain blood and some hemosiderin, the T1 values are shortened, resulting in a decrease in the ADC [21, 22, 28, 49]. The mean ADC of mature cystic teratomas was lower than of malignant ovarian cystic tumors (Figs. 6, 8) [22,23]. The cystic components of mature cystic teratomas usually contain fat. Because DWI with EPI sequences usually uses a fat saturation RF pulse, the low ADC values of the cystic component of mature cystic teratomas have been attributed to artifacts caused by coexisting fat within the tumor [21, 22]. Furthermore, mature cystic teratoma is lined with keratinized squamous epithelium in most cases [23]. The restricted Brownian movement of water molecules within the keratinoid substance results in a high signal on DWI and a low ADC value, which was first utilized in the diagnosis of intracranial epidermoid cyst [50]. Detecting the keratinoid substance by means of DWI and the ADC value may be useful and serve as an adjunctive tool to ensure the accuracy of the diagnosis, particularly in patients with fatless mature cystic teratoma [23]. Among malignant ovarian tumors, the ADC varied widely (Figs. 6, 9), a phenomenon attributable to their morphologic variety [21–23]. The ADC is useful for distinguishing mature cystic teratomas and endometrial cysts from other cystic tumors. However, it is difficult to

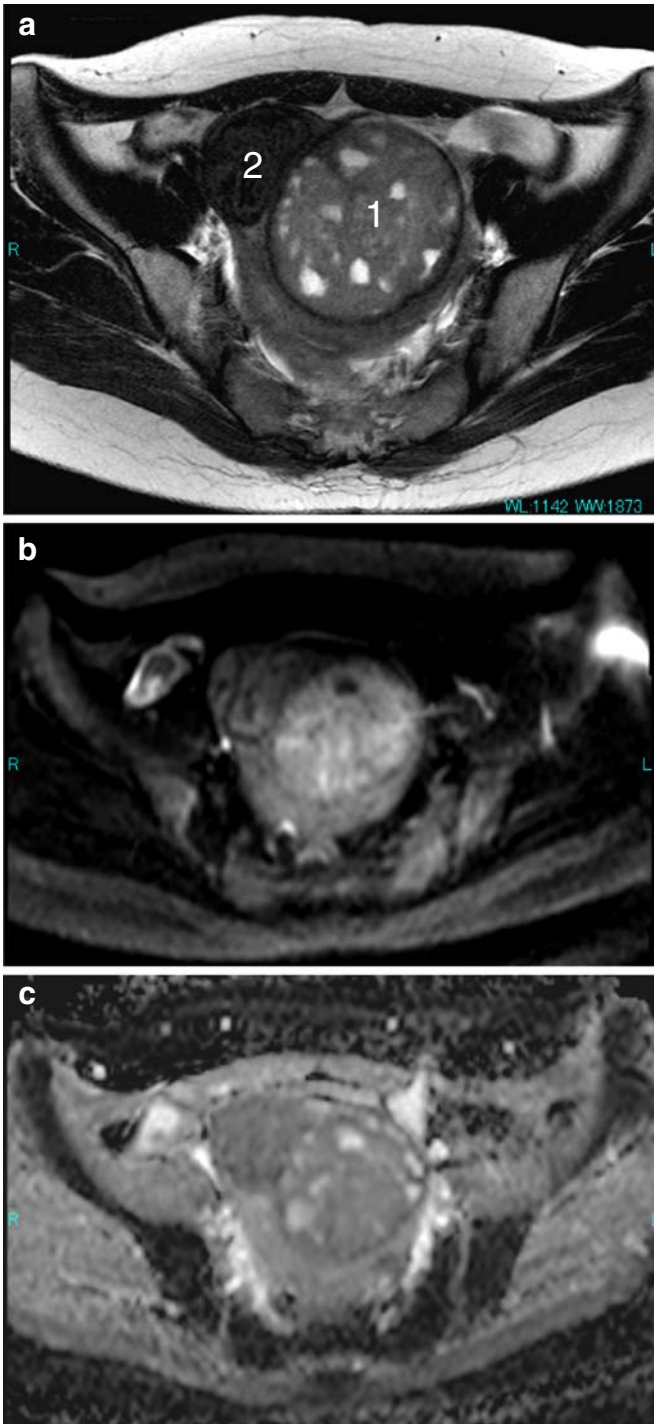

Fig. 5a–c A 32-year-old woman with degenerated (*1*) and ordinary (*2*) leiomyoma of the myometrium. **a** Axial T2-WI shows well-defined myometrial masses as heterogeneous high intensity (*1*) and homogeneous low intensity (*2*). **b** DWI with b = 1,000 s/mm^2 visualizes both masses as heterogeneous hyperintensity. An intermediate signal loss is detected in both leiomyomas. **c** ADC map demonstrates the tumor as a slight hypointensity relative to the normal myometrium. The ADC values within the mass are 1.47×10^{-3} (*1*) and 1.16×10^{-3} mm^2/s (*2*)

identify the ADC threshold for differentiating among cystic ovarian tumors. The role of DWI in distinguishing between benign and malignant cystic tumors may thus be limited [21–23]. The ADC values calculated from the DWI may add useful information to the differential diagnosis of ovarian cystic masses in limited populations, such as those with mature cystic teratomas with a small amount of fat [23]. To our knowledge, the utility of DWI and ADC for solid ovarian tumors has not previously been investigated.

Detection of peritoneal dissemination

The peritoneal cavity is a common site of metastatic spread of gynecological malignancies, especially in patients with ovarian cancer (Figs. 9, 10) [51–56]. The sensitivity and specificity of contrast-enhanced computed tomography (CT) were 85–93% and 78–96%, respectively [52,53]; they were 95% and 80% on contrast-enhanced MRI [54]. Clinically, the detection of peritoneal dissemination is rendered difficult by the poor contrast resolution vis-a-vis surrounding organs. DWI clearly discriminates the abnormal signal intensity of peritoneal dissemination from the signal arising from surrounding organs such as the bowel (Figs. 9, 10). Fujii et al. [57] showed that DWI was highly sensitive (90%) and specific (95.5%) for the evaluation of peritoneal dissemination and was of equal value as contrast-enhanced imaging in gynecological malignancy (n = 26). This technique is also expected to be useful for detecting recurrent gynecological tumors. However, this study population was relatively small, and sensitivity and specificity was measured per patient and not per lesion. A larger prospective study is needed to establish the accuracy of DWI for peritoneal dissemination.

Detection of lymph node metastasis and bone metastasis

The presence of lymph node metastasis is an important issue for patients with gynacological cancers, since it influences the 5-year survival and affects treatment planning [58]. A threshold diameter of 10 mm in the short axis is commonly applied in MRI for distinguishing metastatic from benign nodes, with sensitivity ranging from 24% to 73% [59–61]. It follows that this cutoff cannot be considered completely satisfactory in the evaluation of nodal status in this patient group. Since the highly cellular tissue in reactive lymph nodes may also show increased intensity, the role of DWI and ADC in distinguishing between benign and malignant lymph nodes may be limited. Lin et al. [62] reported the combination of size and relative ADC values was useful in detecting pelvic lymph node metastasis in 50 patients with cervical and uterine cancers (Fig. 11). They showed that the ADC value of the

Table 2 DWI studies with ADC values in ovarian diseases

Authors of Study	Year of Publication	Journal	Tumour & Tissue (no. of subjects)	b-values	ADC (10–3 mm2/s)
Moteki. et al. [21]	2000	J Magn Reson Imaging	Endometrial cyst (33)	2, 188	1.00-1.09 ± 0.57-0.60
			Serous cystadenomas (4)		2.74 ± 0.37
			Mucinous cystadenoma(4)		1.59-1.88 ± 0.89-0.99
			Malignant cystic tumor (12)		1.55-2.00 ± 0.59-1.01
Katayama M. et al. [22]	2002	J Comput Assist Tomogr	Endometrial cyst (18)	200, 400, 600	1.24±0.46
			Mature cystic teratoma (29)		1.27±0.66
			Serous cystadenoma (2)		1.64±0.14
			Mucinous cystadenoma (7)		1.61±0.61
			Malignant cystic tumors (10)		1.64±0.48
Nakayama T. et al. [23]	2005	J Magn Reson Imaging	Endometrial cyst (35)	0, 500, 1000	1.37 ± 0.66
			Imaging Mature cystic teratoma (54)		0.89 ± 0.55
			Benign cystadenoma (14)		2.52 ± 0.32
			Malignant cystic tumors (24)		2.28 ± 0.71

* p<0.01, ** p<0.03

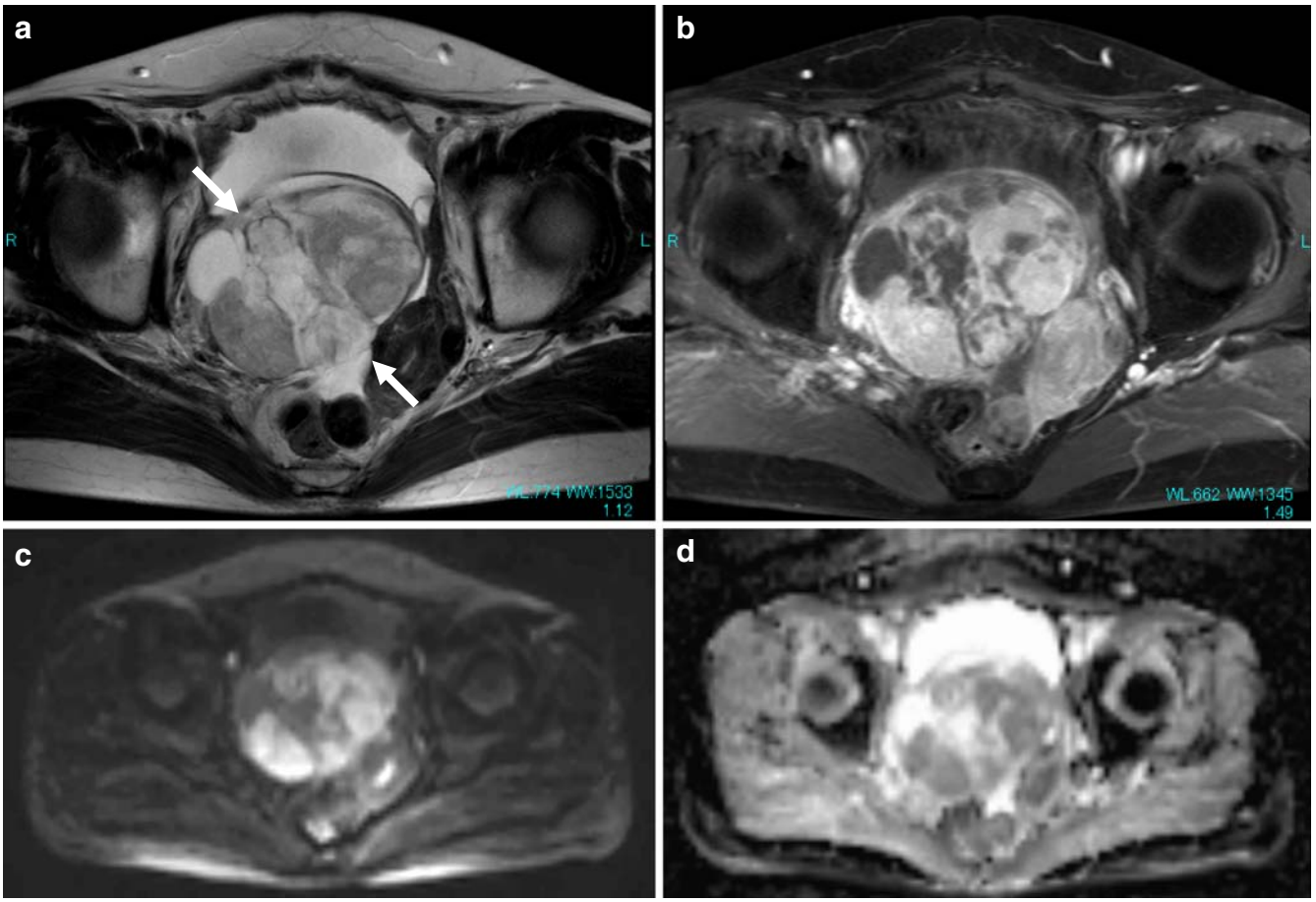

Fig. 6a–d A 60-year-old woman with right ovarian clear cell carcinoma. **a** Axial T2-WI shows a multilocular solid- and cystic mass (*arrows*) with heterogeneous hyperintensity. **b** Post-contrast T1-WI with fat suppression reveals heterogeneous contrast enhancement within the solid component. **c** DWI with b = 1,000 s/mm^2 shows hyperintensity within the solid component. **d** The ADC map demonstrates the tumor as intermediate intensity and urine in the bladder as hyperintensity. The ADC value within the mass is 1.88×10^{-3} mm^2/s

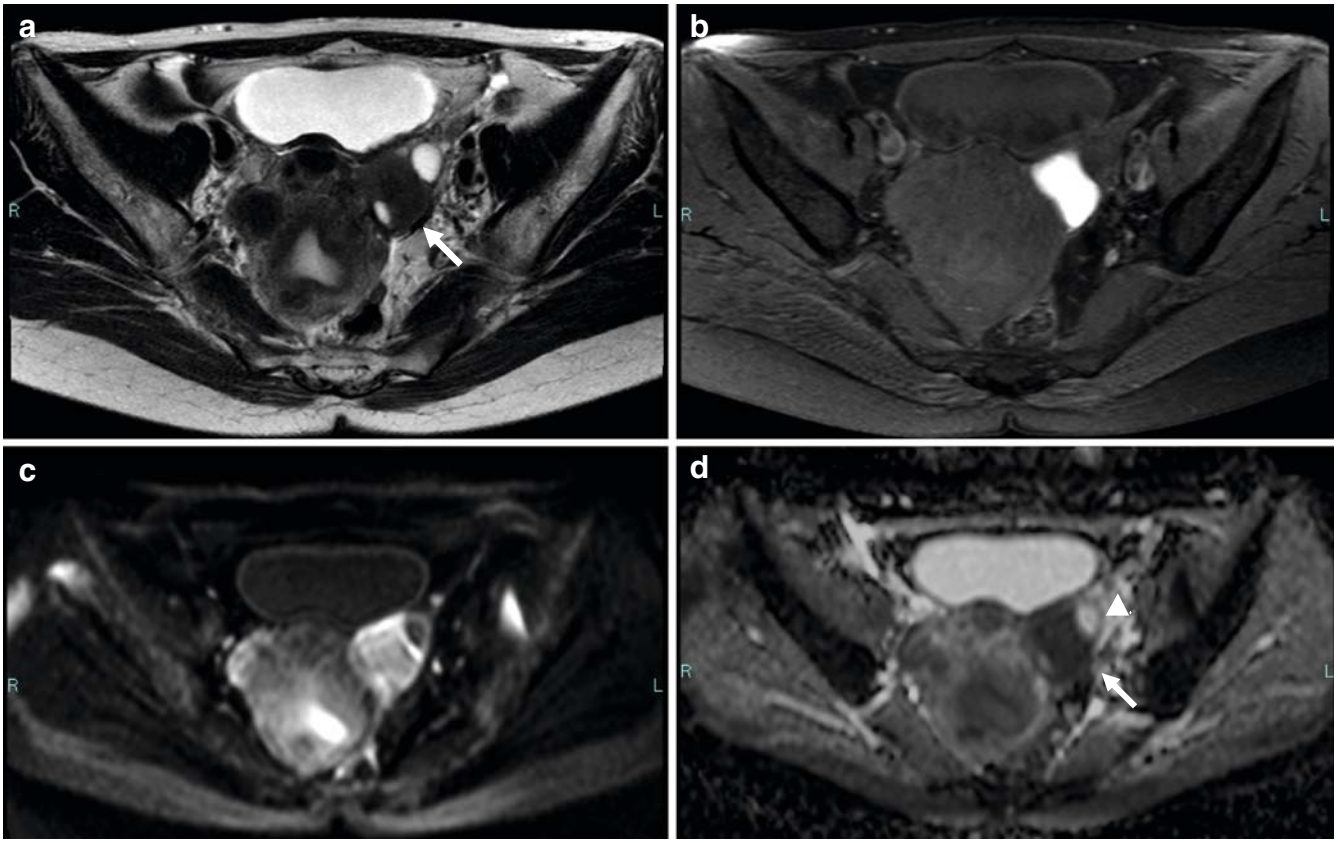

Fig. 7a–d A 46-year-old woman with uterine leiomyomas and a bleeding cyst. **a** Axial T2-WI shows an area of hypointensity in the center of the cystic component (*arrow*). **b** On T1-WI with fat suppression the area in the cystic component is hyperintense. (**c**) On DWI with b = 1,000 s/mm^2 the area in the cystic component is hyperintense. **d** ADC map demonstrates the component as hypointense (*arrow*) and the normal ovary as hyperintense (*arrowhead*). The ADC value within the cystic component is 0.86×10^{-3} mm^2/s

metastatic lymph nodes was higher than that of benign nodes (0.83×10^{-3} vs 0.75×10^{-3} mm^2/s), albeit not significantly. However, the relative ADC values between tumor and nodes were significantly lower in metastatic than in benign nodes (0.06×10^{-3} vs 0.21×10^{-3} mm^2/s: cutoff value 0.10×10^{-3} mm^2/s) (Fig. 11). For the development of the relative ADC criterion, they assumed that regional lymph nodes invaded by tumor cells would display similar cellularity and/or microarchitecture, in a way similar to the primary tumor. The ADC value in the malignant lymph nodes would be similar to that of the primary tumor. Furthermore, they defined that a metastatic lymph node was possible for short axis diameter ≥5 mm with long axis diameter ≥11 mm or a short axis to long axis ratio >0.6 (Fig. 11). Compared with conventional MRI, the method combining size and relative ADC values resulted in better sensitivity (25% vs 83%) and similar specificity (98% vs 99%) with region basis (n = 300). They concluded that the combination of size and relative ADC values was useful in detecting pelvic lymph node metastasis in patients with cervical and uterine cancers. However, the method combining size and relative ADC values was proposed by using a combination of four complicated parameters: ADC of primary tumor, ADC of lymph node, and short- and long-axis diameters of lymph nodes. A larger prospective study with simpler criterion is needed to establish the accuracy of DWI for lymph node metastasis.

To our knowledge, the utility of DWI for metastatic bone tumor from gynecological diseases has not previously been investigated. Moreover, reports of DWI for metastatic bone tumor from other origins are limited [24, 25, 63, 64]. There is controversy regarding the usefulness of DWI for the detection of metastatic bone tumor.

Current status and future directions of DWI for gynecological diseases

Figure 12 shows a decision-making diagram in the MRI diagnosis of gynecological diseases. Both the conventional

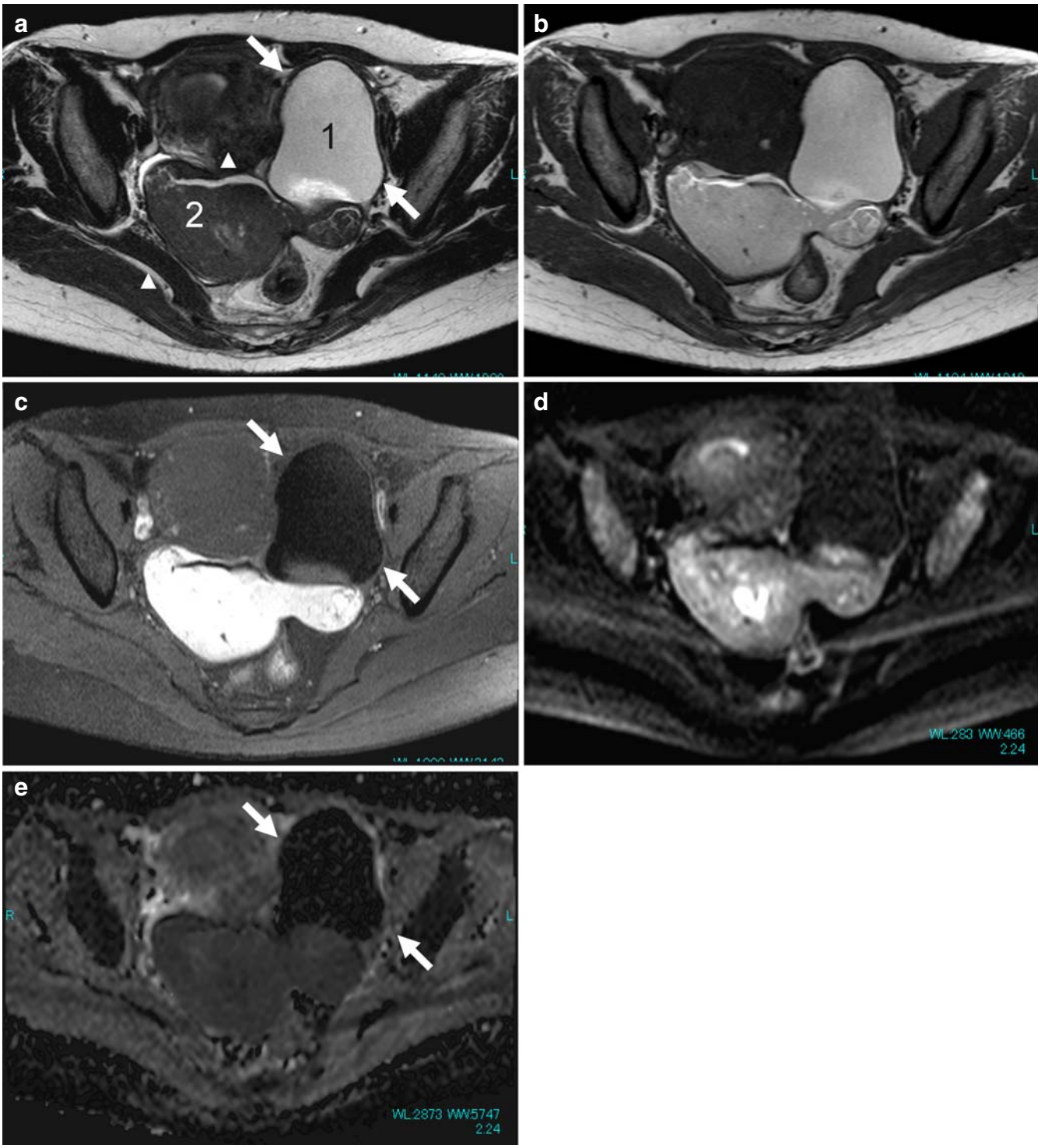

Fig. 8a–e A 46-year-old woman with mature cystic teratoma. **a** Axial T2-WI shows an area of hyperintensity on the anterior cystic component (*1*, *arrows*) and hypointensity on the posterior cystic component (*2*, *arrowheads*). **b** T1-WI shows hyperintensity on both cystic components. **c** T1-WI with fat suppression reveals a marked signal decrease on the anterior cystic component (*1*). **d** DWI with $b = 1{,}000$ s/mm^2 shows marked hypointensity on the anterior cystic component due to fat suppression on the DWI. **e** ADC map demonstrates marked hypointensity (*arrows*) of the anterior cystic component. The ADC values within the cystic components are 0.32×10^{-3} (*1*) and 0.86×10^{-3} mm^2/s (*2*)

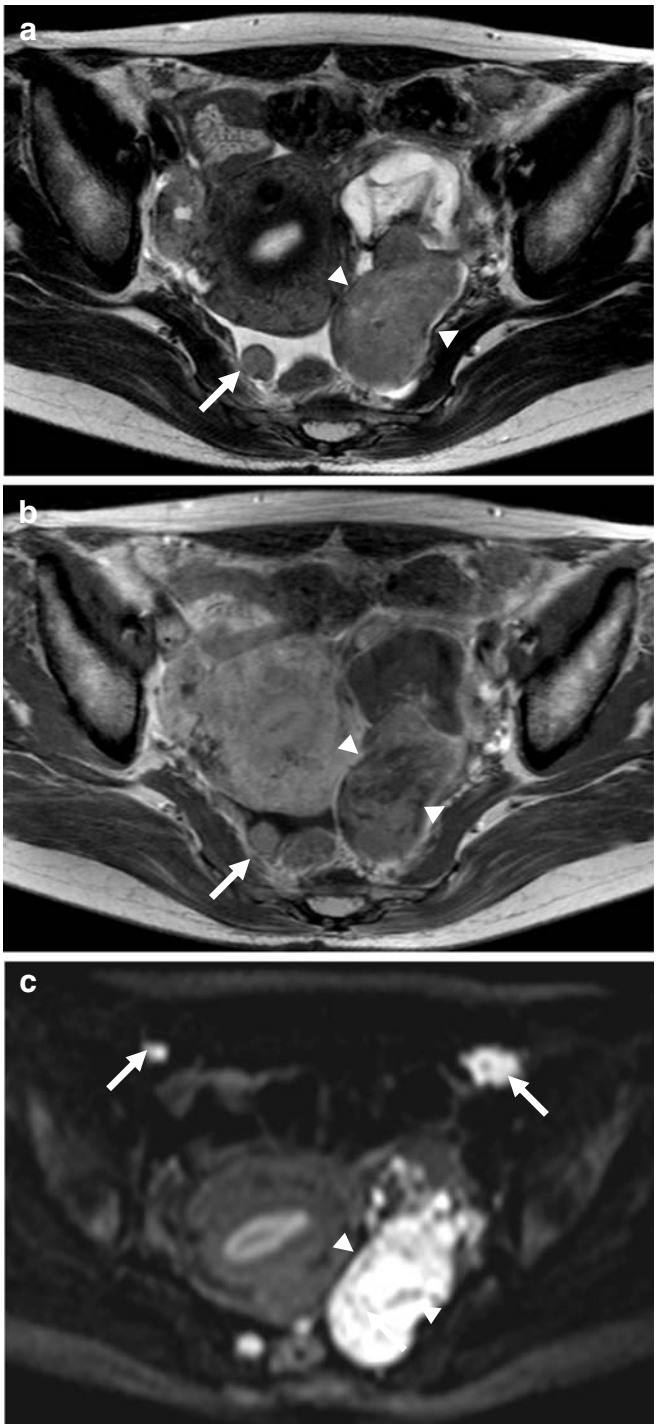

Fig. 9a–c A 49-year-old woman with peritoneal dissemination from ovarian serous adenocarcinoma. T2-WI (**a**) and post-contrast T1-WI (**b**) show a left ovarian cancer (*arrowheads*) and peritoneal disseminated masses (*arrows*). **c** DWI with $b = 1{,}000$ s/mm^2 clearly demonstrates the ovarian cancer (*arrowheads*) and small peritoneal disseminated masses as marked hyperintensity. Small omental masses are difficult to detect on T2-WI and post-contrast images (*white arrows*)

signal intensity characteristics and the ADC of the lesion should be considered to distinguish between benign and malignant gynecological diseases. However, there are some overlaps between benign and malignant gynecocological diseases with using this chart. The ADC may make it possible to differentiate between normal and cancerous tissue in the uterine cervix and endometrium. In the uterine myometrium, the ADC value may play a limited role due to the large overlap between sarcomas and benign leiomyomas. The role of DWI for the differentiation of benign and malignant tumors may be limited in the ovary. Among cystic ovarian lesions, most benign endometrial cysts and mature cystic teratomas had lower ADC values than malignant neoplasms. A combined evaluation of relative ADC values and size criteria improves the preoperative characterization of lymph node metastases compared with conventional MRI. DWI has high sensitivity and specificity for the evaluation of peritoneal dissemination.

DWI can be applied widely for tumor detection and tumor characterization and for the monitoring of response to treatment. Because DWI is an emerging technique, there are few studies on the utility of DWI for gynecological imaging. Thus, further prospective study using larger numbers of patients and long-term follow-up is needed to establish the potential ability of DWI for gynecological diseases. More work is also needed to understand the pathologic changes associated with features observed on DWI. Furthermore, DWI in the gynecological diseases for tumor assessment is the lack of standardization. The techniques applied to acquire DWI, including the choice of *b*-values, vary considerably. Consequently, considerable differences in the ADC values of similar diseases have been reported using different techniques. Clearly, future standardization of protocols for both image acquisition and data analysis across imaging platforms is important. Reproducibility measurements are necessary to determine the limits of error in obtaining quantitative ADC measurements to better understand the magnitude of change that can be confidently detected. Reproducibility is particularly important if DWI measurements are to be routinely used for monitoring therapeutic effects in the future. DWI allows delineation of malignant tumors with excellent conspicuity owing to generally suppressed background noise. However, we consider that it was necessary to refer to other imaging sequences for enough identification of the lesion boundaries because DWI has relative poor spatial resolution. It is still necessary to require administration of intravenous contrast media for assessment of the lesion boundaries and tumor perfusion. For ADC to be used in a clinical setting in gynecological diseases, further study into its predictive value for long-term outcome, along with technical developments to minimize spatial distortion and demonstration of reproducible measurements will be required.

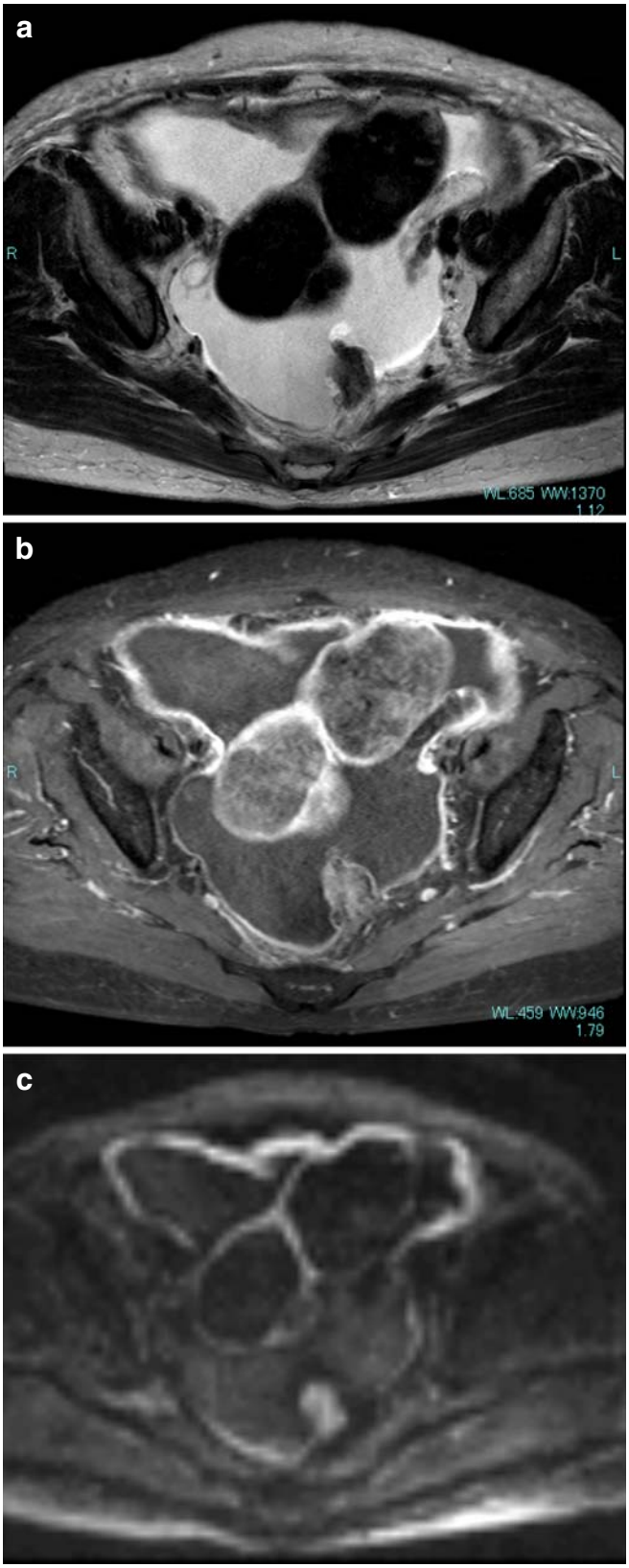

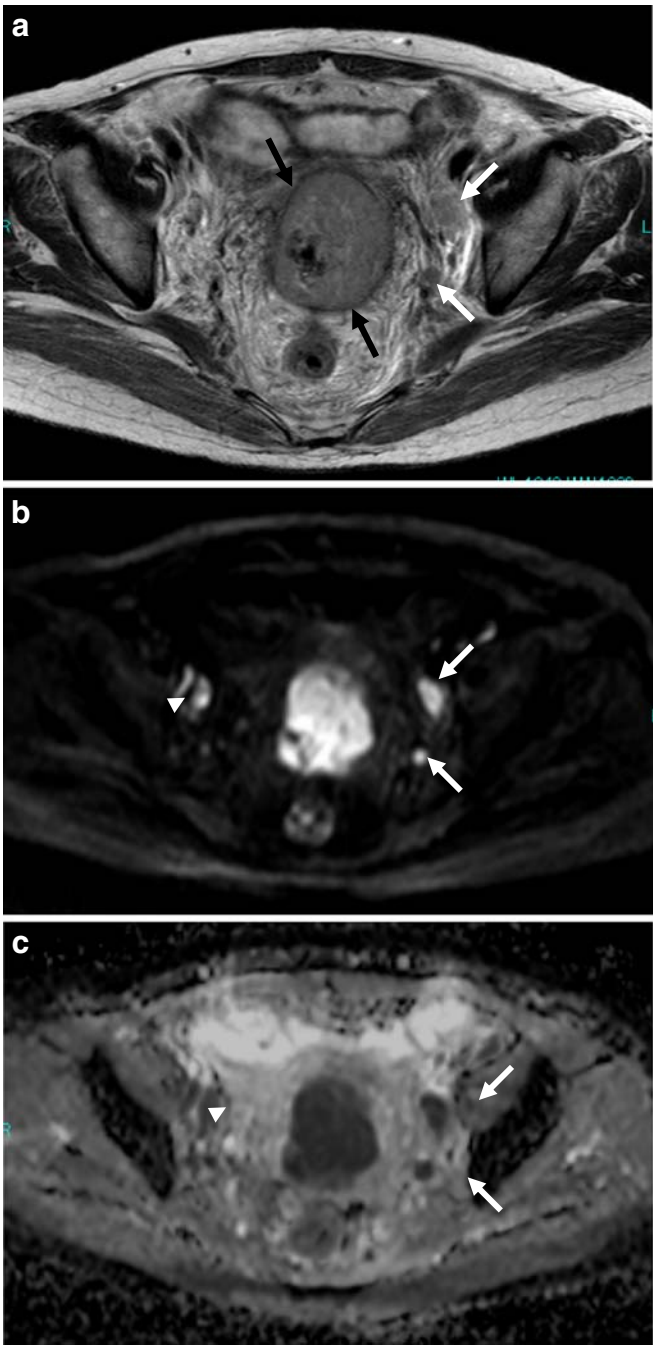

◀ **Fig. 10a–c** A 67-year-old woman with peritoneal dissemination from an ovarian serous adenocarcinoma. **a** On T2-WI it is difficult to detect peritoneal dissemination. **b** Post-contrast T1-WI shows peritoneal enhancement in the uterovesical space and posterior cul-de-sac. **c** DWI clearly depicts peritoneal dissemination as marked hyperintensity. For the evaluation of peritoneal dissemination, DWI and post-contrast images with fat suppression are of equal value

◀ **Fig. 11a–c** A 69-year-old woman with squamous cell carcinoma of the uterine cervix with multiple lymph node metastases. **a** Axial T2-WI of the uterus shows cervical cancer (*black arrow*) with multiple lymph node metastases (*white arrow*). **b** DWI with $b = 1{,}000$ s/mm^2 clearly demonstrates the cervical cancer with metastatic (*arrows*) and reactive (*arrowhead*) lymph nodes as marked hyperintensity. Small lymph nodes are difficult to detect on T2-WI. **c** On the ADC map, the tumor and lymph nodes are hypointense. Lymph nodes are noted in the external iliac region (*arrows* and *arrowhead*). The left anterior and posterior nodes are 13 mm in the short axis, 20 mm in the long axis and 6 mm in the short axis, 7-mm in long axis, respectively (*arrows*). The absolute ADC values of both lymph nodes are 0.77×10^{-3} and 0.73×10^{-3} mm^2/s, and the ADC value of uterine cervical tumor is 0.71×10^{-3} mm^2/s; therefore, the relative ADC values are 0.06×10^{-3} and 0.02×10^{-3} mm^2/s, respectively. These lymph nodes are predicted as metastases. Another lymph node is noted in the right (*arrowhead*). The absolute ADC value of the lymph node is 0.95×10^{-3} mm^2/s; therefore, the relative ADC value is 0.22×10^{-3} mm^2/s. This lymph node is predicted as reactive node

Conclusions

In combination with conventional MRI, DWI and ADC findings provide additional information in patients with gynecological diseases. We found that the combination of DWI and conventional MRI identified additional sites of pelvic tumors and improved the radiologist's confidence in image interpretation. Additional advantages of DWI include its completely noninvasive nature and its cost-effectiveness. DWI does not involve radiation exposure, the oral or intravenous administration of contrast material, and does not elicit patient discomfort. DWI can be easily added to MR study protocols and loses no time to the injection of contrast material. DWI may play an important role in the diagnosis and follow-up of patients with gynecological diseases.

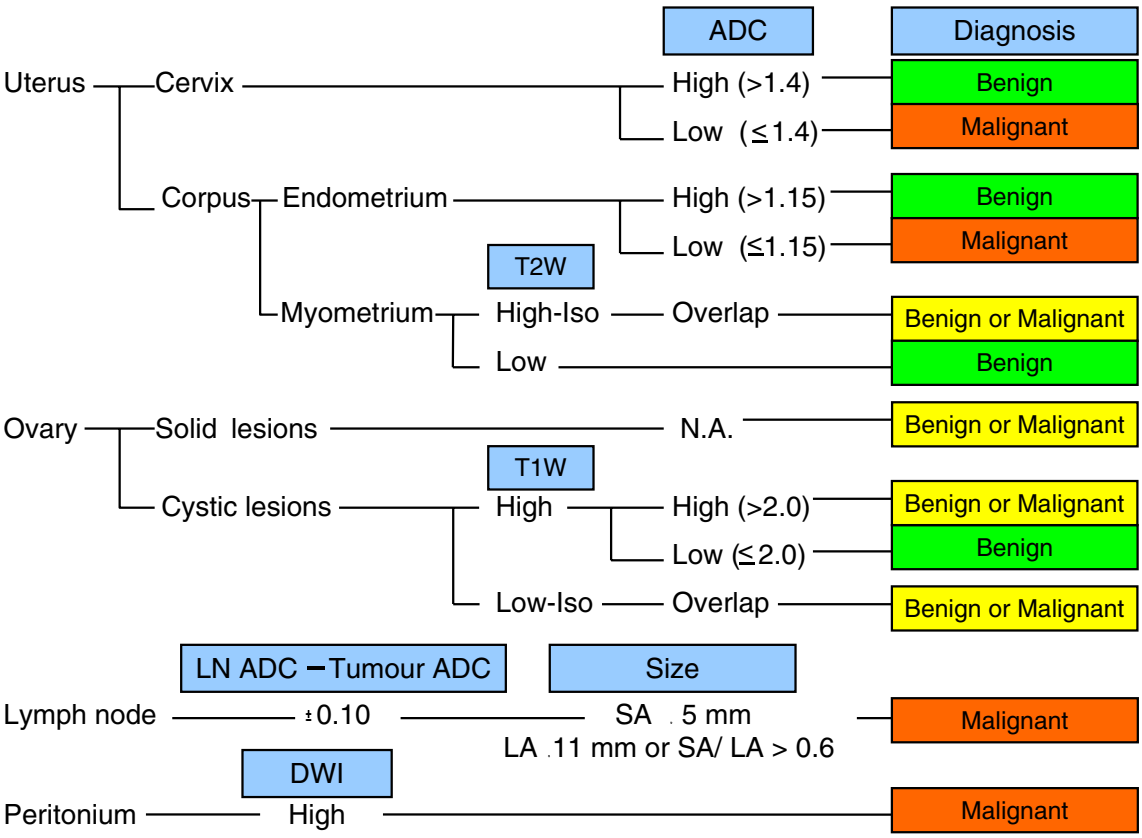

Fig. 12 Flow chart of MRI diagnosis of gynecological diseases. Note some overlaps between benign and malignant gynecocological diseses with using this chart (*LN* lymph node, *SA* short axis of the lymph node, *LA* long axis)

References

1. Le Bihan D, Breton E, Lallemand D, Grenier P, Cabanis E, Laval-Jeantet M (1986) MR imaging of intravoxel incoherent motions: application to diffusion and perfusion in neurologic disorders. Radiology 161:401–407
2. Li TQ, Takahashi AM, Hindmarsh T, Moseley ME (1999) ADC mapping by means of a single-shot spiral MRI technique with application in acute cerebral ischemia. Magn Reson Med 41:143–147
3. Schaefer PW, Grant PE, Gonzalez RG (2000) Diffusion-weighted MR imaging of the brain. Radiology 217:331–345
4. Kurihara Y, Yakushiji YK, Tani I, Nakajima Y, Van Cauteren M (2002) Coil sensitivity encoding in MR imaging: advantages and disadvantages in clinical practice. AJR Am J Roentgenol 178:1087–1091
5. Namimoto T, Yamashita Y, Sumi S, Tang Y, Takahashi M (1997) Focal liver masses: characterization with diffusion-weighted echo-planar MR imaging. Radiology 204:739–744
6. Ichikawa T, Haradome H, Hachiya J, Nitatori T, Araki T (1998) Diffusion weighted MR imaging with a single-shot echoplanar sequence: detection and characterization of focal hepatic lesions. AJR Am J Roentgenol 170:397–402
7. Sato C, Naganawa S, Nakamura T et al (2005) Differentiation of noncancerous tissue and cancer lesions by apparent diffusion coefficient values in transition and peripheral zones of the prostate. J Magn Reson Imaging 21:258–262
8. Charles-Edwards EM, deSouza NM (2006) Diffusion-weighted magnetic resonance imaging and its application to cancer. Cancer Imaging 6:135–143
9. Hosseinzadeh K, Schwarz SD (2004) Endorectal diffusion-weighted imaging in prostate cancer to differentiate malignant and benign peripheral zone tissue. J Magn Reson Imaging. 20:654–661
10. Matoba M, Tonami H, Kondou T, Yokota H, Higashi K, Toga H, Sakuma T (2007) Lung carcinoma: diffusion-weighted MR imaging-preliminary evaluation with apparent diffusion coefficient. Radiology 243:570–577
11. Theilmann RJ, Borders R, Trouard TP, Xia G, Outwater E, Ranger-Moore J, Gillies RJ, Stopeck A (2004) Changes in water mobility measured by diffusion MRI predict response of metastatic breast cancer to chemotherapy. Neoplasia 6:831–837
12. Naganawa S, Sato C, Kumada H, Ishigaki T, Miura S, Takizawa O (2005) Apparent diffusion coefficient in cervical cancer of the uterus: comparison with the normal uterine cervix. Eur Radiol 15:71–78
13. McVeigh PZ, Syed AM, Milosevic M, Fyles A, Haider MA (2008) Diffusion-weighted MRI in cervical cancer. Eur Radiol 18:1058–1064
14. Tamai K, Koyama T, Saga T, Umeoka S, Mikami Y, Fujii S, Togashi K (2007) Diffusion-weighted MR imaging of uterine endometrial cancer. J Magn Reson Imaging 26:682–687
15. Fujii S, Matsusue E, Kigawa J, Sato S, Kanasaki Y, Nakanishi J, Sugihara S, Kaminou T, Terakawa N, Ogawa T (2008) Diagnostic accuracy of the apparent diffusion coefficient in differentiating benign from malignant uterine endometrial cavity lesions: initial results. Eur Radiol 18:384–389
16. Shen SH, Chiou YY, Wang JH, Yen MS, Lee RC, Lai CR, Chang CY (2008) Diffusion-weighted single-shot echo-planar imaging with parallel technique in assessment of endometrial cancer. AJR Am J Roentgenol 190:481–488
17. Tamai K, Koyama T, Saga T, Morisawa N, Fujimoto K, Mikami Y, Togashi K (2008) The utility of diffusion-weighted MR imaging for differentiating uterine sarcomas from benign leiomyomas. Eur Radiol 18:723–730
18. Jacobs MA, Herskovits EH, Kim HS (2005) Uterine fibroids: diffusion weighted MR imaging for monitoring therapy with focused ultrasound surgery-preliminary study. Radiology 236:196–203
19. Liapi E, Kamel IR, Bluemke DA, Jacobs MA, Kim HS (2005) Assessment of response of uterine fibroids and myometrium to embolization using diffusion-weighted echoplanar MR imaging. J Comput Assist Tomogr 29:83–86
20. Shimada K, Ohashi I, Kasahara I, Watanabe H, Ohta S, Miyasaka N, Itoh E, Shibuya H (2004) Differentiation between completely hyalinized uterine leiomyomas and ordinary leiomyomas: three-phase dynamic magnetic resonance imaging (MRI) vs. diffusion weighted MRI with very small b-factors. J Magn Reson Imaging 20:97–104
21. Moteki T, Ishizaka H (2000) Diffusion-weighted EPI of cystic ovarian lesions: evaluation of cystic contents using apparent diffusion coefficients. J Magn Reson Imaging 12:1014–1019
22. Katayama M, Masui T, Kobayashi S, Ito T, Sakahara H, Nozaki A, Kabasawa H (2002) Diffusion-weighted echo planar imaging of ovarian tumors: is it useful to measure apparent diffusion coefficients? J Comput Assist Tomogr 26:250–256
23. Nakayama T, Yoshimitsu K, Irie H, Aibe H, Tajima T, Nishie A, Asayama Y, Matake K, Kakihara D, Matsuura S, Nakano H, Honda H (2005) Diffusion-weighted echo-planar MR imaging and ADC mapping in the differential diagnosis of ovarian cystic masses: usefulness of detecting keratinoid substances in mature cystic teratomas. J Magn Reson Imaging 22:271–278
24. Koyama T, Togashi K (2007) Functional MR imaging of the female pelvis. J Magn Reson Imaging 25:1101–1112
25. Koyama T, Tamai K, Togashi K (2006) Current status of body MR imaging: fast MR imaging and diffusion-weighted imaging. Int J Clin Oncol 11:278–285
26. Thoeny HC, De Keyzer F (2007) Extracranial applications of diffusion-weighted magnetic resonance imaging. Eur Radiol 17:1385–1393
27. Provenzale JM, Engelter ST, Petrella JR, Smith JS, MacFall JR (1999) Use of MR exponential diffusion-weighted images to eradicate T2 “shine-through” effect. AJR Am J Roentgenol 172:537–539
28. Silvera S, Oppenheim C, Touzé E, Ducreux D, Page P, Domigo V, Mas JL, Roux FX, Frédy D, Meder JF (2005) Spontaneous intracerebral hematoma on diffusion-weighted images: influence of T2-shine-through and T2-blackout effects. AJNR Am J Neuroradiol 26:236–241
29. Yamashita Y, Takahashi M, Sawada T, Miyazaki K, Okamura H (1992) Carcinoma of the cervix: dynamic MR imaging. Radiology 182:643–648
30. Hirano Y, Kubo K, Hirai Y, Okada S, Yamada K, Sawano S, Yamashita T, Hiramatsu Y (1992) Preliminary experience with gadolinium-enhanced dynamic MR imaging for uterine neoplasms. Radiographics 12:243–256

31. Yamashita Y, Harada M, Torashima M, Takahashi M, Miyazaki K, Tanaka N, Okamura H (1996) Dynamic MR imaging of recurrent postoperative cervical cancer. J Magn Reson Imaging 6:167–171
32. Tsuda K, Murakami T, Kurachi H, Ogawa H, Oi H, Miyake A, Narumi Y, Nakamura H (1997) MR imaging of cervical carcinoma: comparison among T2-weighted, dynamic, and postcontrast T1-weighted images with histopathological correlation. Abdom Imaging 22:103–107
33. Nicolet V, Carignan L, Bourdon F, Prosmanne O (2000) MR imaging of cervical carcinoma: a practical staging approach. Radiographics 20:1539–1549
34. Kinkel K (2006) Pitfalls in staging uterine neoplasm with imaging: a review. Abdom Imaging 31:164–173
35. Yamashita Y, Harada M, Sawada T, Takahashi M, Miyazaki K, Okamura H (1993) Normal uterus and FIGO stage I endometrial carcinoma: dynamic gadolinium-enhanced MR imaging. Radiology 186:495–501
36. Takahashi S, Murakami T, Narumi Y, Kurachi H, Tsuda K, Kim T, Enomoto T, Tomoda K, Miyake A, Murata Y, Nakamura H (1998) Preoperative staging of endometrial carcinoma: diagnostic effect of T2-weighted fast spin-echo MR imaging. Radiology 206:539–547
37. Manfredi R, Gui B, Maresca G, Fanfani F, Bonomo L (2005) Endometrial cancer: magnetic resonance imaging. Abdom Imaging 30:626–636
38. Sahdev A, Sohaib SA, Jacobs I, Shepherd JH, Oram DH, Reznek RH (2001) MR imaging of uterine sarcomas. AJR Am J Roentgenol 177:1307–1311
39. Goto A, Takeuchi S, Sugimura K, Maruo T (2002) Usefulness of Gd-DTPA contrast-enhanced dynamic MRI and serum determination of LDH and its isozymes in the differential diagnosis of leiomyosarcoma from degenerated leiomyoma of the uterus. Int J Gynecol Cancer 12:354–361
40. Tanaka YO, Nishida M, Tsunoda H, Okamoto Y, Yoshikawa H (2004) Smooth muscle tumors of uncertain malignant potential and leiomyosarcomas of the uterus: MR findings. J Magn Reson Imaging 20:998–1007
41. Koyama T, Togashi K, Konishi I, Kobayashi H, Ueda H, Kataoka ML, Itoh T, Higuchi T, Fujii S, Konishi J (1999) MR imaging of endometrial stromal sarcoma: correlation with pathologic findings. AJR Am J Roentgenol 173:767–772
42. Ueda M, Otsuka M, Hatakenaka M, Torii Y (2000) Uterine endometrial stromal sarcoma located in uterine myometrium: MRI appearance. Eur Radiol 10:780–782
43. Ueda M, Otsuka M, Hatakenaka M, Sakai S, Ono M, Yoshimitsu K, Honda H, Torii Y (2001) MR imaging findings of uterine endometrial stromal sarcoma: differentiation from endometrial carcinoma. Eur Radiol 11:28–33
44. Hricak H, Tscholakoff D, Heinrichs L et al (1986) Uterine leiomyomas: correlation of MR, histopathologic findings, and symptoms. Radiology 158:385–391
45. Ueda H, Togashi K, Konishi I, Kataoka ML, Koyama T, Fujiwara T, Kobayashi H, Fujii S, Konishi J (1999) Unusual appearances of uterine leiomyomas: MR imaging findings and their histopathologic backgrounds. Radiographics 19:S131–S145
46. Yamashita Y, Torashima M, Takahashi M, Tanaka N, Katabuchi H, Miyazaki K, Ito M, Okamura H (1993) Hyperintense uterine leiomyoma at T2-weighted MR imaging: differentiation with dynamic enhanced MR imaging and clinical implications. Radiology 189:721–725
47. Spies JB, Roth AR, Jha RC et al (2002) Leiomyoma treated with uterine artery embolization: factors associated with successful symptom and imaging outcome. Radiology 222:45–52
48. Smart OC, Hindley JT, Regan L, Gedroyc WM (2006) Magnetic resonance guided focused ultrasound surgery of uterine fibroids-the tissue effects of GnRH agonist pre-treatment. Eur J Radiol 592:163–167
49. Maldjian JA, Listerud J, Moonis G, Siddiqi F (2001) Computing diffusion rates in T2-dark hematomas and areas of low T2 signal. AJNR Am J Neuroradiol 22:112–118
50. Chen S, Ikawa F, Kurisu K, l, Arita K, Takaba J, Kanou Y (2001) Quantitative MR evaluation of intracranial epidermoid tumors by fast fluid-attenuated inversion recovery imaging and echo-planar diffusion-weighted imaging. AJNR Am J Neuroradiol 22:1089–1096
51. Kurtz AB, Tsimikas JV, Tempany CM, Hamper UM, Arger PH, Bree RL, Wechsler RJ, Francis IR, Kuhlman JE, Siegelman ES, Mitchell DG, Silverman SG, Brown DL, Sheth S, Coleman BG, Ellis JH, Kurman RJ, Caudry DJ, McNeil BJ (1999) Diagnosis and staging of ovarian cancer: comparative values of Doppler and conventional US, CT, and MR imaging correlated with surgery and histopathologic: report of the Radiology Diagnostic Oncology Group. Radiology 212:19–27
52. Tempany CM, Zou KH, Silverman SG, Brown DL, Kurtz AB, McNeil BJ (2000) Staging of advanced ovarian cancer: comparison of imaging modalities-report from the Radiological Diagnostic Oncology Group. Radiology 215:761–767
53. Coakley FV, Choi PH, Gougoutas CA, Pothuri B, Venkatraman E, Chi D, Bergman A, Hricak H (2002) Peritoneal metastases: detection with spiral CT in patients with ovarian cancer. Radiology 223:495–499
54. Ricke J, Sehouli J, Hach C, Hanninen EL, Lichtenegger W, Felix R (2003) Prospective evaluation of contrastenhanced MRI in the depiction of peritoneal spread in primary or recurrent ovarian cancer. Eur Radiol 13:943–949
55. Pannu HK, Horton KM, Fishman EK (2003) Thin section dual-phase multidetector-row computed tomography detection of peritoneal metastases in gynecologic cancers. J Comput Assist Tomogr 27:333–340
56. Pannu HK, Bristow RE, Montz FJ, Fishman EK (2003) Multidetector CT of peritoneal carcinomatosis from ovarian cancer. Radiographics 23:687–701
57. Fujii S, Matsusue E, Kanasaki Y, Kanamori Y, Nakanishi J, Sugihara S, Kigawa J, Terakawa N, Ogawa T (2008) Detection of peritoneal dissemination in gynecological malignancy: evaluation by diffusion-weighted MR imaging. Eur Radiol 18:18–23
58. Lutman CV, Havrilesky LJ, Cragun JM, Secord AA, Calingaert B, Berchuck A, Clarke-Pearson DL, Soper JT (2006) Pelvic lymph node count is an important prognostic variable for FIGO stage I and II endometrial carcinoma with high-risk histology. Gynecol Oncol 102:92–97

59. Yu KK, Hricak H, Subak LL, Zaloudek CJ, Powell CB (1998) Preoperative staging of cervical carcinoma: phased array coil fast spin-echo versus body coil spin-echo T2-weighted MR imaging. AJR Am J Roentgenol 171:707–711
60. Reinhardt MJ, Ehritt-Braun C, Vogelgesang D, Ihling C, Högerle S, Mix M, Moser E, Krause TM (2001) Metastatic lymph nodes in patients with cervical cancer: detection with MR imaging and FDG PET. Radiology 218:776–782
61. Rockall AG, Sohaib SA, Harisinghani MG, Babar SA, Singh N, Jeyarajah AR, Oram DH, Jacobs IJ, Shepherd JH, Reznek RH (2005) Diagnostic performance of nanoparticle-enhanced magnetic resonance imaging in the diagnosis of lymph node metastases in patients with endometrial and cervical cancer. J Clin Oncol 23:2813–2821
62. Lin G, Ho KC, Wang JJ, Ng KK, Wai YY, Chen YT, Chang CJ, Ng SH, Lai CH, Yen TC (2008) Detection of lymph node metastasis in cervical and uterine cancers by diffusion-weighted magnetic resonance imaging at 3T. J Magn Reson Imaging 28:128–135
63. Castillo M, Arbelaez A, Smith JK, Fisher LL (2000) Diffusion-weighted MR imaging offers no advantage over routine noncontrast MR imaging in the detection of vertebral metastases. AJNR Am J Neuroradiol 21:948–953
64. Nakanishi K, Kobayashi M, Nakaguchi K, Kyakuno M, Hashimoto N, Onishi H, Maeda N, Nakata S, Kuwabara M, Murakami T, Nakamura H (2007) Whole-body MRI for detecting metastatic bone tumor: diagnostic value of diffusion-weighted images. Magn Reson Med Sci 6:147–155